PREDICTIVE SIMULATION IN ATMOSPHERIC VEHICLE ENTRY: RADIATION MODEL DEVELOPMENT

André Maurente, maurente@ices.utexas.edu
Institute for Computational Engineering and Sciences, The University of Texas at Austin
John Howell, jhowell@mail.utexas.edu
Department of Mechanical Engineering, Cockrell School of Engineering, The University of Texas at Austin

Paul T. Bauman, pbauman@ices.utexas.edu
Kenji Miki, kenji@ices.utexas.edu
Jeremy Jagodzinski, jags@ices.utexas.edu
Ernesto Prudencio, prudenci@ices.utexas.edu
Serge Prudhomme, serge@ices.utexas.edu
Roy H. Stogner, roystgnr@ices.utexas.edu
Institute for Computational Engineering and Sciences, The University of Texas at Austin

Abstract. *During hypersonic entry of a vehicle into Earth's atmosphere, as the air speed changes from hypersonic to subsonic, kinetic energy is suddenly converted into thermal energy, rapidly increasing the temperature of the air across the shock layer and promoting chemical dissociation, partial ionization, and thermodynamic nonequilibrium. At such conditions the air around the spacecraft emits considerable amounts of radiative energy so that a significant portion of the overall heat flux to the vehicle surface is due to radiation. Furthermore, radiation heat transfer throughout the shock layer highly influences the flowfield and therefore the convective heat flux to the vehicle surface. The recession rate of the Thermal Protection System (TPS) depends on the total heat flux to the vehicle surface. Thus accurate predictive simulation of coupled radiation-flow-chemistry is essential to perform TPS sizing. The goal of this work is to present an overview about a radiation model and its coupling with a hypersonic flow-chemistry solver for predictive entry simulation.*

Keywords: Vehicle entry; radiation heat transfer; radiation-flow-chemistry coupled simulation

1. INTRODUCTION

1.1 Motivation

Entry of large blunt vehicles (capsules) into Earth's atmosphere exhibits various coupled and complex physical phenomena at multiple spatial and temporal scales. A strong bow shock is created upstream of the vehicle that suddenly converts part of the kinetic energy of the air into internal energy. The temperature of the air around the vehicle can reach values higher than ten thousand of degrees Kelvin. This rapid heating promotes nonequilibrium conditions, chemical dissociation, and partial ionization of the air into a plasma. This high temperature air plasma emits considerable amounts of radiation and transfers heat to the vehicle surface by convection and radiation. To survive this extreme heating, a Thermal Protection System (TPS) is applied to the surface of the vehicle. Most TPS employ an ablative heat shield of complex micro/nano-scale composite materials. A quantity of engineering interest for the design of TPS is the so-called recession rate, which provides a measure of the rate at which the protective system is ablated.

Ground-based experiments do not allow complete experimental observation of the complex physics relative to flight conditions and flight tests are expensive, so that data available from them are limited, and they can only sample a small fraction of the possible trajectories and flight conditions. Further, the cost of a failure during entry is high. Thus, predictive simulation is of great interest for both design and operational decision making. The goals of this work are to present a simple radiation model aimed at entry simulation as well as its coupling with a hypersonic flow-chemistry solver.

1.2 General Entry Physics and Entry Simulation

Figure 1 depicts a capsule with a nose diameter of 5 m, designed to bring back to Earth four to six astronauts. For such a large blunt vehicle, in a lunar return trajectory, the peak heating period occurs at an altitude around 60 km, and lasts approximately 60 s. During this peak heating period, the vehicle can experience Mach numbers between 20 and 45, and thus the energy flux to the vehicle surface as well as the recession rate of the TPS are maxima. To predict the recession rate of the TPS material, it is necessary to develop and solve a multiphysics system of equations that describe coupled chemical and thermodynamic nonequilibrium, hypersonic flow, radiation heat transfer and ablation processes.
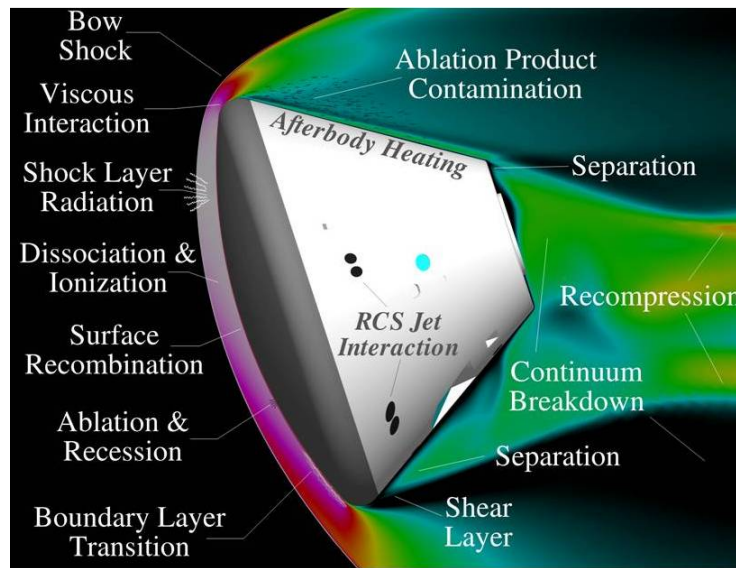
Figure 1. Schematic of a space capsule and list of physical phenomena occuring during atmospheric entry.

2. THE RADIATION MODEL

The air plasma within the shock layer of an entry vehicle is mainly constituted of N_2, N, N^+, O_2, O, O^+, NO, NO^+ and free electrons, which can dissociate, ionize and recombine. The plasma through these processes usually emit considerable radiation. In addition, ablation of the TPS material introduces carbon and hydrogen into the surrounding air, which react with the existing species to give new constituents such as C, C^+, CO, CO_2, C_2, C_3, CN, H, H^+ and H_2. The molecules, atoms, ions and free electrons composing the gas can be at various energy levels. According to the quantum mechanical description, the molecules and atoms can be in specific bound electronic, vibrational, and rotational energy levels. A bound-bound transition occurs when an atom or molecule moves from one bound energy state to another, emitting or absorbing a photon with a specific frequency that is related to the amount of energy necessary to cause the transition. It follows that the emitted and absorbed radiation contains discrete spectral lines and exhibits very irregular wavelength dependence. However the spectral lines have a finite spectral width resulting from various line broadening effects. In bound-free transitions, an atom or molecule absorbs a photon with sufficient energy to cause ionization, or a free electron and an ion combine emitting a photon. A free-free transition occurs when a free electron passes near an ion and interacts with its electrical magnetic field without being captured into a bound state. Both bound-free and free-free transitions are associated with continuous spectra since the free electron can have any amount of energy. Because the different thermochemical processes have different relaxation times, part of the shock layer in most reentry conditions is in non-local thermodynamic equilibrium condition. At non-local thermodynamic equilibrium the absorption and emission are not proportional and the radiative transfer equation is given as

$$\frac{dI_\lambda(s)}{ds} = \eta_\lambda(\phi) - \kappa_\lambda(\phi)I_\lambda(s) \tag{1}$$

where s is the coordinate along a given line, $I_\lambda = I_\lambda(s)$, is the spectral intensity, ϕ is a vector that contains the medium properties that affect the emission coefficient, $\eta_\lambda = \eta_\lambda(\phi)$, as well as the absorption coefficient, $\kappa_\lambda = \kappa_\lambda(\phi)$. The state vector ϕ depends on the location s in the medium, that is, $\phi = \phi(s)$. The boundary condition for Eq. (1) is the prescribed intensity of radiation, $I_{\lambda,w}$, given at the boundary of the problem domain (here, the subscript w refers to a wall, for instance, the surface of a space vehicle).

The spectra shown in Fig. 2, which simulate radiation from an early NASA entry experiment (FIRE II), indicate that the emission and absorption of radiative energy is strongly dependent on the wavelength. These spectra are computed at only one point in the shock layer and at a specific flight time. At different locations and flight times, the temperature, pressure, and chemical composition can considerably vary resulting in different spectral properties. Therefore, computing the medium properties and the line-by-line integration for the radiation heat transfer, is computationally extremely expensive, making it necessary to use simplified radiation models. Our objective is always to use the simplest and cheapest models that would provide accurate results. In this work, we choose a simple radiation model and plan to evaluate whether the model is reliable for entry simulations.

According to Bose et al., 2008, the air plasma during the peak of radiation heat transfer for a large capsule entering Earth's atmosphere is almost fully dissociated into oxygen and nitrogen atoms and ions with high levels of ionization (one
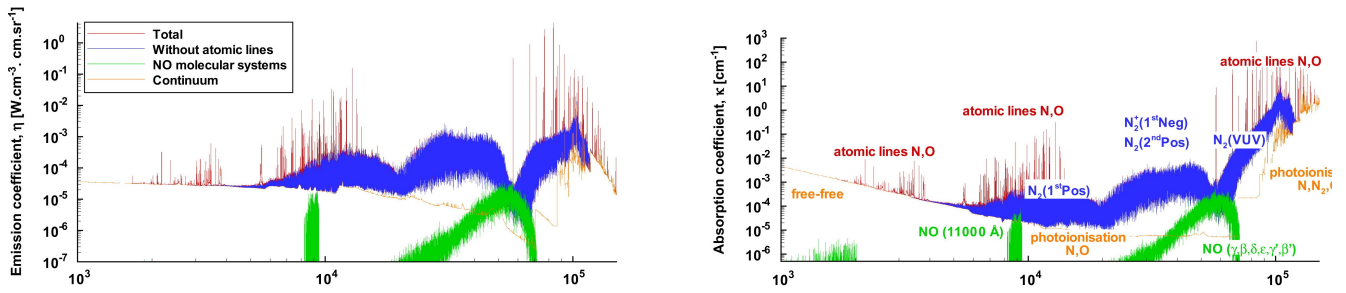
Figure 2. Emission and absorption coefficients for a point in the shock layer of FIRE II at flight time equal to 1,642 seconds [Lamet et al., 2008].

to five percent) and most of the shock layer is in local-thermodynamic equilibrium. We make the assumption that the air plasma is a gray gas in local-thermodynamic equilibrium and with uniform composition. Because the thickness of the shock layer is small compared to the nose diameter of the vehicle, the variation of temperature and radiative properties is considerably higher in the direction normal to the surface of the vehicle than in the tangent direction. Therefore we choose to adopt the tangent slab approximation for the radiation heat transfer model. This approximation reduces the model to a one-dimensional model, which is applied to compute the radiation exchange along each line normal to the vehicle surface. The following sections 2.1 and 2.2 present the gray gas model and tangent slab approximation.

2.1 Gray gas model

The gray gas model makes the assumption that the absorption coefficient is independent of the wavelength. The radiation heat transfer equation for a gray gas is

$$\frac{dI(s)}{ds} = a(\phi)I_b(T) - a(\phi)I(s) \tag{2}$$

where $I = I(s)$ is the total intensity and $T = T(s)$ is the local temperature of the medium. For the case of a gray gas the state vector, $\phi = \phi(s)$, contains only the local temperature and pressure. The boundary condition for Eq. (2) is a given intensity, I_w, at the boundary of the domain and the local blackbody intensity, $I_b(T)$ is given by:

$$I_b(T) = \frac{\sigma T^4}{\pi} \tag{3}$$

where σ is the Stefan-Boltzmann constant.

In the gray gas model, the absorption coefficient is a spectrally averaged value over all wavelengths. Approximation methods to derive averaged values of the absorption coefficient are presented by Siegel and Howell, 2002, and Modest, 2003. In our model, the absorption coefficient of the gray gas is averaged based on the total intensity of radiation, I_{sp}. The subscript sp is used to indicate that the intensity I_{sp} is not computed with Eq. (2), but is provided from SPECAIR (Laux, 2002), a code that features spectroscopic nonequilibrium models. We use the following formula to compute the mean absorption coefficient with respect to the local properties of the medium:

$$a(\phi) = \frac{-1}{\delta s} \ln \left(1 - \frac{I_{sp}}{I_b(T)} \right) \tag{4}$$

where the total intensity, I_{sp}, depends on the solution of Eq. (1) along the path length δs for all wavelengths and integration over the spectrum. The emission and absorption coefficients are evaluated at the medium conditions, characterized by the state vector, which for a uniform medium is constant along the path length, $\phi(s) = constant$. In the case of a gray gas it is usual to assume that the absorption coefficient only depends on temperature and pressure. Moreover, we assume here that the medium is composed of nitrogen and oxygen atoms with five percent ionization level, which is representative of plasmas encountered in the shock layer of large entry vehicles. Thus, the only variables are temperature and pressure and so the state vector can be expressed as $\phi = (T, P)$. The value of $\delta s = 30$ cm was selected as it is approximately the shock layer thickness during entry, at the peak of the radiative heat transfer.

In order to avoid excessive storage, we choose to curve fit the absorption coefficient of the gray gas data. This fitting, which provides the absorption coefficient as a function of the state vector, $\phi = (T, P)$, is given by:

$$f(P) = c_{p,1}P^3 + c_{p,2}P^2 + c_{p,3}P + c_{p,4} \tag{5}$$

$$a(\phi) = f(P)(c_{t,1}T^4 + c_{t,2}T^3 + c_{t,3}T^2 + c_{t,4}T + c_{t,5}) \tag{6}$$

where the constant parameters $c_{p,i}$, $i = 1, 2, 3$ and 4, and $c_{t,j}$, $j = 1, 2, 3, 4$ and 5 are determined following the approach presented in section 3.

2.2 Tangent slab approximation

Figure 3 describes the tangent slab approximation. This figure shows the temperature field in a hypersonic flow, associated with a Mach number of 31, around a cylindrical body. This result was computed with a hypersonic flow solver coupled with the radiation model presented here. The line L_1, normal to the vehicle surface (Fig. 3 (a)), is the stagnation line. To compute the radiation heat transfer along this line by applying the tangent slab approximation, one can assume a plane slab of medium as represented in Fig. 3 (b), which is infinite in two directions and finite in the direction normal to the surface of the body. The temperature and radiative properties along the slab vary only in the direction of the line L_1. Therefore, the one-dimensional radiation heat transfer, Eq. (2), is solved in the slab along L_1. Upon choosing a different line, e.g., L_2 in Fig. 3 (a), a new slab is defined in which Eq. (2) is solved to obtain the radiation heat transfer.
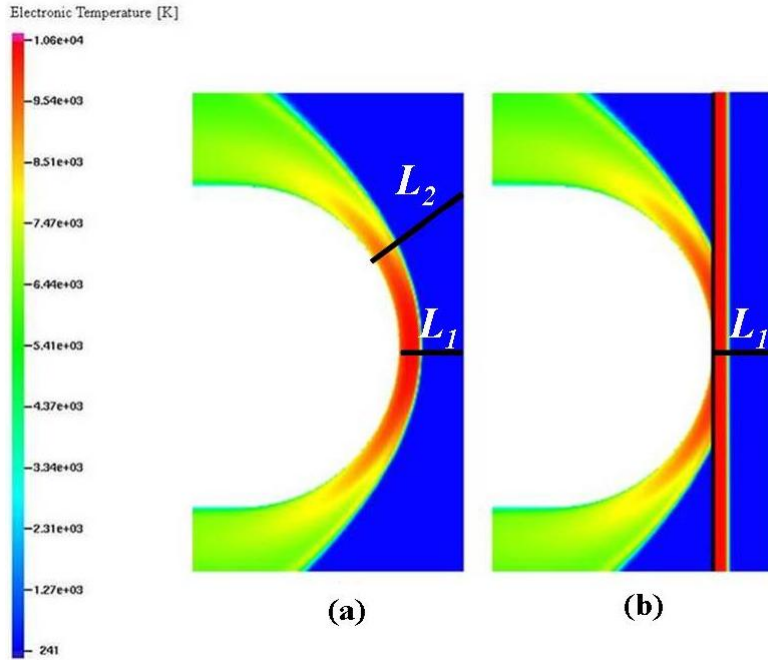
Figure 3. Distribution of temperature in a hypersonic flow around a cylindrical body (simulated with a hypersonic flow solver coupled to the radiation code).

Figure 4 shows the one-dimensional geometry of a plane slab. It consists of a medium confined between two infinite parallel walls. The slab is uniform, that is, isothermal and homogeneous, along the infinite directions and non-uniform along the finite direction. All paths s for the radiation intensity originate at the left or right boundary. As shown in Fig. 4, the path direction is given by the angle θ measured from the positive z direction. The superscripts $+$ and $-$ correspond to the positive and negative directions of $\cos \theta$, respectively, so that I^+ corresponds to $0 \leq \theta \leq \pi/2$ and I^- corresponds to $\pi/2 \leq \theta \leq \pi$. The relation between the s and z directions is

$$s = \frac{z}{\cos \theta} \tag{7}$$

For the positive and negative z directions, the radiative transfer equation, Eq. (2), becomes

$$\cos \theta \, \frac{\partial I^+}{\partial z} = -a(\phi)I^+(z,\theta) + a(\phi)I_b(T), \qquad \text{for } 0 \leq \theta \leq \pi/2 \tag{8}$$

$$\cos \theta \, \frac{\partial I^-}{\partial z} = -a(\phi)I^-(z,\theta) + a(\phi)I_b(T), \qquad \text{for } \pi/2 \leq \theta \leq \pi \tag{9}$$

Equations (8) and (9) are integrated subjected to the following boundary conditions:

$$I^+(0,\theta) = I_w^+(\theta) \tag{10}$$
$$I^-(D,\theta) = I_w^-(\theta) \tag{11}$$

In the case of entry the intensities in Eq. (10) and Eq. (11) are the blackbody intensity at the vehicle surface and zero at the boundary located at the cold universe. Integration of Eq. (8) and Eq. (9) subjected to the boundary conditions
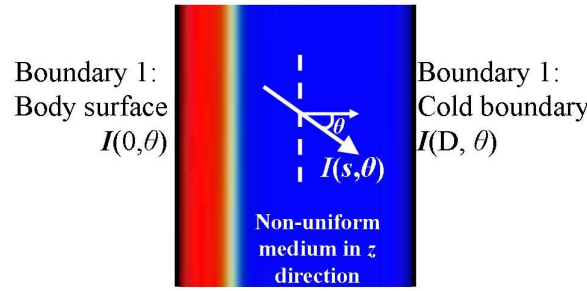
Figure 4. One-dimensional plane slab of medium.

Eq. (10) and Eq. (11) gives the intensities as a function of location and angle in the slab:

$$I^+(z, \theta) = I_w^+(\theta) \exp\left(-\frac{1}{\cos\theta}\int_0^z a(\phi)dz'\right)$$

$$+ \frac{1}{\cos\theta}\int_0^z I_b(z')\exp\left(-\frac{1}{\cos\theta}\int_{z'}^z a(\phi)dz^*\right)dz', \qquad \text{for } 0 \le \theta \le \pi/2 \tag{12}$$

$$I^-(z, \theta) = I_w^-(\theta) \exp\left(\frac{1}{\cos\theta}\int_z^D a(\phi)dz'\right)$$

$$- \frac{1}{\cos\theta}\int_z^D I_b(z')\exp\left(\frac{1}{\cos\theta}\int_z^{z'} a(\phi)dz^*\right)dz', \qquad \text{for } \pi/2 \le \theta \le \pi \tag{13}$$

The net radiative heat flux in the positive z direction crossing dA in the plane at z in Fig. 4 consists of two contributions, one from I^+ and one from I^-. Since intensity is energy per unit solid angle crossing an area normal to the direction of I, the projection of dA must be considered normal to either I^+ or I^-. The energy flux in the positive and negative direction is given by (using $d\omega = 2\pi \sin\theta d\theta$)

$$q_r^+(z) = 2\pi \int_0^{\pi/2} I^+(z, \theta)\cos\theta\sin\theta d\theta \tag{14}$$

$$q_r^-(z) = -2\pi \int_{\pi/2}^{\pi} I^-(z, \theta)\cos\theta\sin\theta d\theta \tag{15}$$

The net radiative heat flux is then

$$q_r(z) = [q_r^+(z) - q_r^-(z)] = 2\pi\left[\int_0^{\pi/2} I^+(z, \theta)\cos\theta\sin\theta d\theta - \int_{\pi/2}^{\pi} I^-(z, \theta)\cos\theta\sin\theta d\theta\right] \tag{16}$$

Substituting the intensities in Eq. (16) by the expressions given in Eq. (12) and Eq. (13), we get:

$$q_r(z) = 2\pi\left\{\int_0^{\pi/2} I_w^+(\theta)\exp\left(-\frac{1}{\cos\theta}\int_0^z a(\phi)dz'\right)\cos\theta\sin\theta d\theta\right.$$

$$- \int_{\pi/2}^{\pi} I_w^-(\theta)\exp\left(\frac{1}{\cos\theta}\int_z^D a(\phi)dz'\right)\cos\theta\sin\theta d\theta$$

$$+ \int_0^{\pi/2}\int_0^z\left[I_b(z')\exp\left(-\frac{1}{\cos\theta}\int_{z'}^z a(\phi)dz^*\right)dz'\right]\sin\theta d\theta$$

$$\left.- \int_{\pi/2}^{\pi}\int_z^D\left[I_b(z')\exp\left(\frac{1}{\cos\theta}\int_z^{z'} a(\phi)dz^*\right)dz'\right]\sin\theta d\theta\right\} \tag{17}$$

The divergence of the radiative heat flux is needed as a source in the energy equation for the hypersonic flow solution. For

a slab with uniform conditions over each boundary, the heat flux depends only on z so that

$$\nabla \cdot q_r(z) = \frac{dq_r(z)}{dz} = 4\pi a(z)I_b(z) - 2\pi a(z)\left\{ \int_0^{\pi/2} \left[I_w^+(\theta) \exp\left(-\frac{1}{\cos\theta}\int_0^z a(\phi)dz' \right) \right. \right.$$
$$\left. + \frac{1}{\cos\theta}\int_0^z I_b(z') \exp\left(-\frac{1}{\cos\theta}\int_{z'}^z a(\phi)dz^* \right)dz' \right] \sin\theta d\theta$$
$$- \int_{\pi/2}^{\pi} \left[I_w^-(\theta) \exp\left(\frac{1}{\cos\theta}\int_z^D a(\phi)dz' \right) \right.$$
$$\left. \left. - \frac{1}{\cos\theta}\int_z^D I_b(z') \exp\left(\frac{1}{\cos\theta}\int_z^{z'} a(\phi)dz^* \right)dz' \right] \sin\theta d\theta \right\} \quad (18)$$

2.3 Result of coupled simulation

Figure 5 shows the translational temperature distribution around an axisymmetric capsule with a nose diameter of 5 m, at a given instance of an entry trajectory at approximately Mach 21. The computational cost of the radiation code in this simulation was insignificant compared to that of the flow solution. Further savings could be achieved by applying the radiation model only to the shock layer region, as the radiative flux have a negligible impact on the energy equation elsewhere.
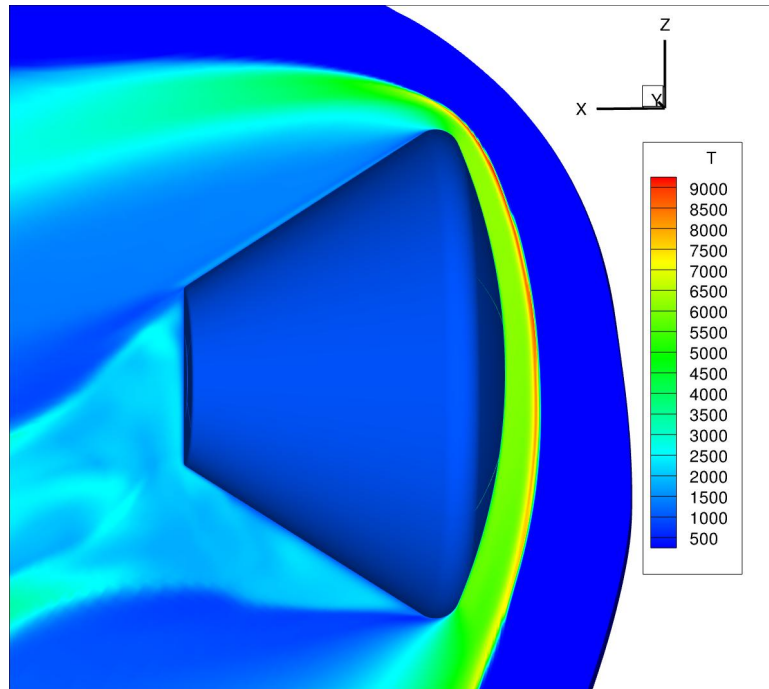
Figure 5. Distribution of the translational temperature in a hypersonic flow around an entry capsule (simulated with hypersonic flow solver and radiation code).

3. SHOCK TUBE SIMULATION

As experimental data for vehicle entry are scarce (flight testing is expensive and can only sample a small fraction of the possible trajectories and flight conditions), shock tube experimental data will be used for evaluating the radiation model. However, the gray gas model is applied only for the transport energy computation and cannot reproduce the spectral signature measured in shock tube testing. Thus, the radiation model was coupled with a chemistry-flow solver and a spectroscopic code (SPECAIR), for shock tube simulation. Fig. 7 shows the shock tube experimental setting. As the shock wave propagates, the air in the shock tube is heated at very high temperatures, becoming an air plasma. The emitted radiation spectrum is measured and information about temperature, pressure, and chemistry fields are inferred based on the spectral signature.

In our shock tube simulation, the radiation model is used only for the computation of the heat flux. The latter influences the temperature, pressure, and chemistry, that in turn affect the spectrum generated by SPECAIR. For validating the
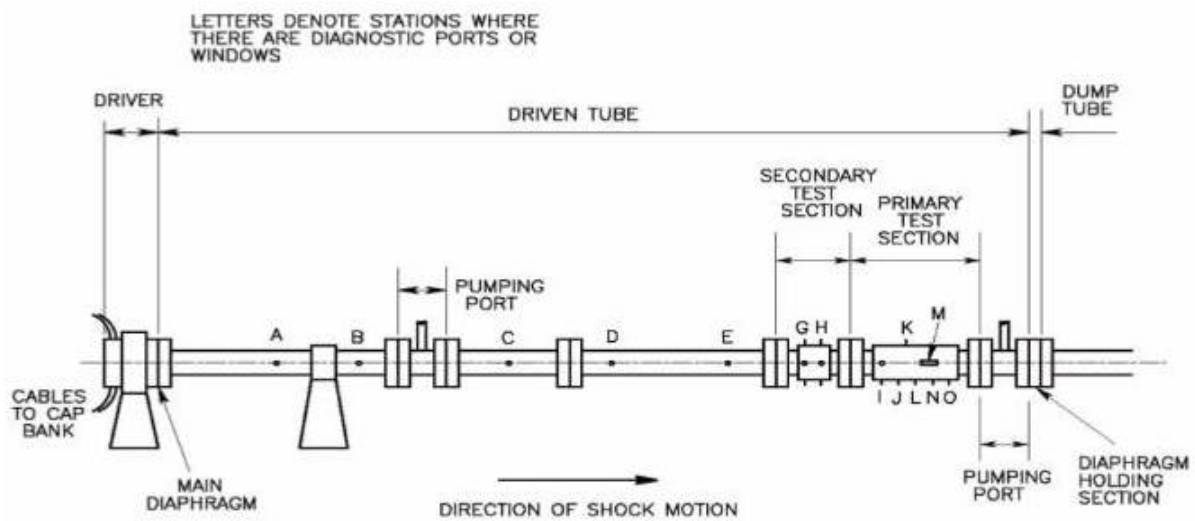
Figure 6. Shock tube experimental setting [Grinstead et al. 2008].

radiation model the spectrum obtained from SPECAIR are compared with shock tube experimental data from NASA's EAST facility. Figures 7 and 8 show the results for the integrated radiation intensity over specific spectral ranges obtained from shock tube experimental data and shock tube simulation, which were presented by Johnston (2008). The data presented in Fig. 7 and Fig. 8 correspond to free stream speed and pressure of 9980 m/s and 40 Pa and of 10340 m/s and 40 Pa, which are representative of conditions occurring in vehicle entry. These shock tube experimental data will later be used to validate the radiation model as a reliable model for entry simulation by applying a calibration/validation framework based on uncertainty quantification of the model predictions.
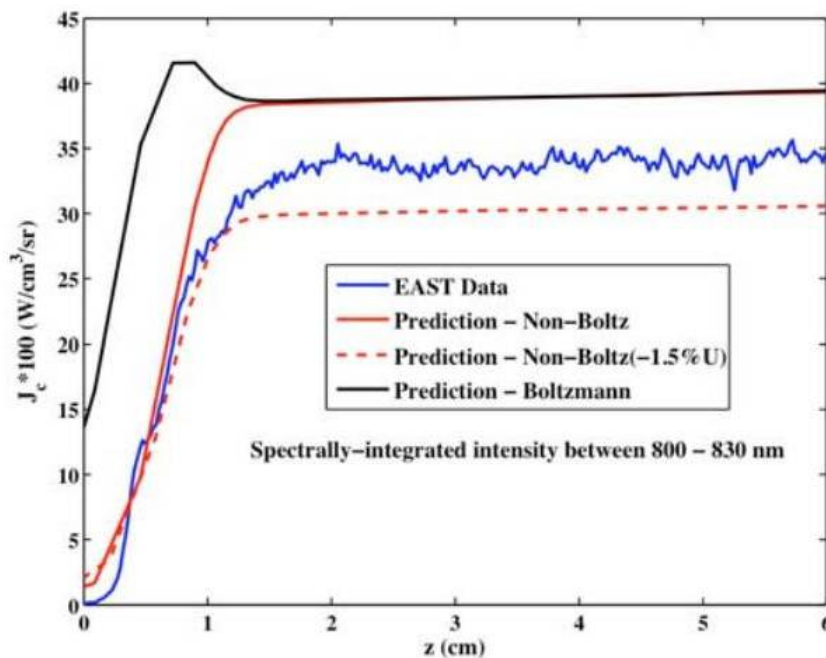
Figure 7. Spatial variation of normalized intensity integrated over the 800-830 nm wavelength range [Johnston, 2008].
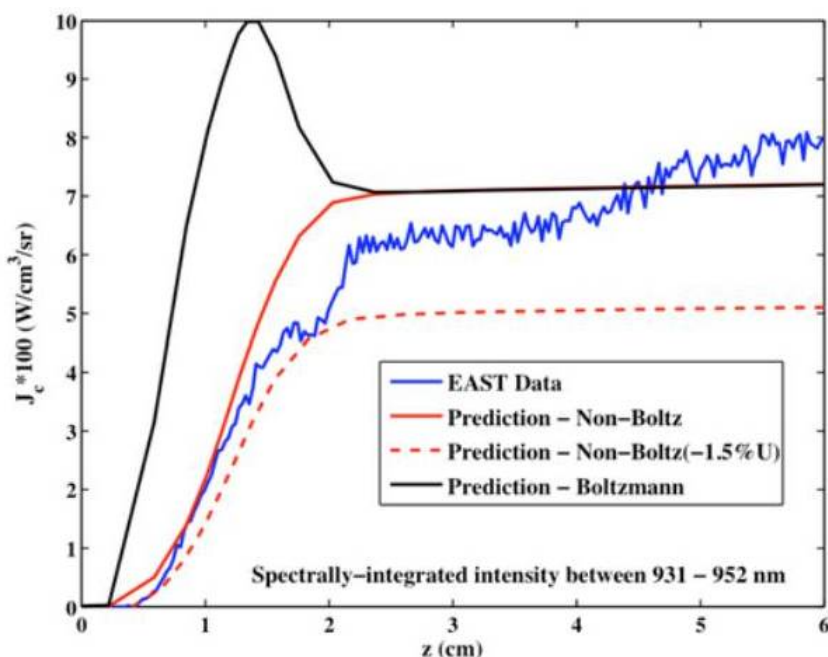
Figure 8. Spatial variation of normalized intensity integrated over the 931-952 nm wavelength range [Johnston, 2008].

4. CONCLUSIONS

Experimental data for vehicle entry are obviously scarce since flight test are expensive and ground experiments do not allow complete observation of the complex physical phenomena occurring during a spatial vehicle entry. Therefore, computer simulations of vehicle entry are crucially needed for both design and operational decision-making. We have described a simple radiation model coupled with a hypersonic flow model for vehicle entry simulation.

5. REFERENCES

Bose, D., McCorkle, E., Thompson, C., Bogdanoff, Prabhu, D., Allen, G., Grinstead, J., 2008 "Analysis and Model Validation of Shock Layer Radiation in Air", 46th AIAA Aerospace Sciences Meeting and Exhibit, 7–10 January, Reno, Nevada, 2008.

Grinstead, J. H. Wilder, M. C., Olejniczak, J., Bogdanoff, D. W., Allen, G. A., Dang, K. and Forrest, M. J., 2008 "Shock-heated Air Radiation Measurements at Lunar Return Conditions", 46th AIAA Aerospace Sciences Meeting and Exhibit, 7–10 January, Reno, Nevada, 2008.

Johnston, C., 2008, "A Comparison of East Shock-Tube Data with a New Air Radiation Model", 46th AIAA Aerospace Sciences Meeting and Exhibit, 7 -10 January, Reno, Nevada, 2008.

Lamet, J., Babou, Y., Rivière, P., Perrin, M., Soufiani, A., 2008, "Radiative transfer in gases under thermal and chemical nonequilibrium conditions: Application to earth atmosphere. ESA workshop, 2008. re-entry", J. of Quantitative Spectroscopy and Radiative Transfer, Vol. 109, pp. 235-244.

Laux, C. O., 2002, "Radiation and Nonequilibrium Collisional-Radiative Models", von Karman Institute Lecture Series 2002-07. Fletcher, D., Charbonnier, J. M., Sarma, G. S. R., and Magin T., eds., Rhode-Saint-Genèse, Belgium, 2002. (program available at http://www.specair-radiation.net/)

Modest, M., 2003, "Radiation Heat Transfer", J. of Quantitative Spectroscopy and Radiative Transfer, Taylor and Francis, New York.

Siegel, R. and Howell, J., 2002, "Thermal Radiation Heat Transfer", Taylor and Francis, New York.

6. ACKNOWLEDGMENT

7. RESPONSIBILITY NOTICE

The authors are the only responsible for the printed material included in this paper